CHARACTERIZATION OF STRUCTURE AND LUMINESCENCE OF TITANIA NANOTUBES

M. Enachi[1], V. Trofim[1], V. Coseac[2], I.M. Tiginyanu[1, 3], and V.V. Ursaki[3]

[1]Technical University of Moldova, 168, Stefan cel Mare ave., MD-2004, Chisinau, Republic of Moldova
[2]Academy of Transport, Informatics, and Communications, 121a, Muncesti str., MD-2002, Chisinau, Moldova
[3]Institute of Applied Physics, Academy of Sciences of Moldova, 5, Academiei str., MD-2028, Chisinau, Republic of Moldova
(Received 25 September 2008)

Abstract

The morphology, structural, and optical properties of porous titania layers prepared by electrochemical oxidation of Ti foils are studied as a function of technological conditions of preparation and post-electrochemical-oxidation thermal treatment. Ti foils were anodized in aqueous and non-aqueous HF and H_3PO_4 solutions by applying various anodizing conditions. Titania nanotubes with diameters ranging from 30 nm to 250 nm with controlled length have been prepared. The influence of thermal treatment upon the structural properties of TiO_2 nanotubes was investigated by means of X-ray diffraction analysis and Raman scattering. It was found that the as prepared samples are amorphous. As the annealing temperature increases to 300°C, an anatase structure is formed. Starting from 500°C, a rutile structure is produced which coexists with the anatase structure. A complete phase transition to the rutile structure occurs at 800°C. The luminescence from both anatase and rutile phases was observed at low temperatures. The origin of luminescence bands is discussed.

1. Introduction

Titania (TiO_2) is widely used as a pigment [1, 2], in sensors [3-5], electrocatalysis [6], and Graetzel-type solar cells [7]. Titania has three polymorphs: anatase, brookite, and rutile. All are constructed with $Ti–O_6$ octahedra and differ only in their octahedral linkage. In anatase, four of twelve octahedral edges are shared with neighboring octahedral; in brookite, three; in rutile, two octahedral share edges [8]. Although rutile is the thermodynamically stable form of titania, generally anatase, and occasionally brookite, crystallizes first during synthesis. Anatase starts to transform to rutile at >600°C [9]. The different crystalline structures of titania have different material properties including density, index of refraction, and catalytic properties.

Recently, titania also gained interest as a material used in photonic band gap crystals for the visible spectrum of light due to its high index of refraction ($n_{rutile} \approx 2.9$) [10] and low absorption [11, 12]. Electrochemical oxidation of Ti foils allows one to prepare a variety of porous titania structures, therefore, enlarging the area of TiO_2 applications in optoelectronic and photonic devices [13]. Taking into account the possibility of doping porous titania templates with rare earth and transition metal ions and the morphology controlled light scattering properties, one can expect that luminescent materials prepared on porous TiO_2 templates are promising for random laser applications.

In this work, we investigate the morphology, structural and, optical properties of porous titania layers as a function of technological conditions of preparation and post-electrochemical-oxidation thermal treatment. For this purpose, technological conditions for the preparation of porous TiO_2 layers with controlled morphology and porosity on the basis of Ti foils were developed.

2. Technological aspects and morphology characterization

Technological conditions for the preparation of porous TiO_2 layers with controlled morphology and porosity on the basis of Ti foils (Aldrich) include rinsing and sonicating in isopropyl alcohol, drying, and anodizing. The samples were anodized in aqueous HF solutions with various additives. Morphologies in the form of arrays of nanotubes were produced. The optimum concentration of the electrolyte was found to be 0.5 wt %. It was found that, by applying various anodizing conditions, it is possible to control the diameter and the length of nanotubes. The diameter of nanotubes increases monotonously from 30 to 100 nm with the voltage increasing from 5 to 30 V at fixed treatment duration of 30 min (see Fig. 1). At the same time, the length of nanotubes increases from 70 nm to 400 nm. The geometrical parameters of the produced structures are also controlled by the duration of anodization. The increase of the anodization duration from 3 min to 30 min at constant voltage of 10 V results in the increase in the nanotube diameter from 30 to 60 nm and the length from 70 nm to 200 nm.

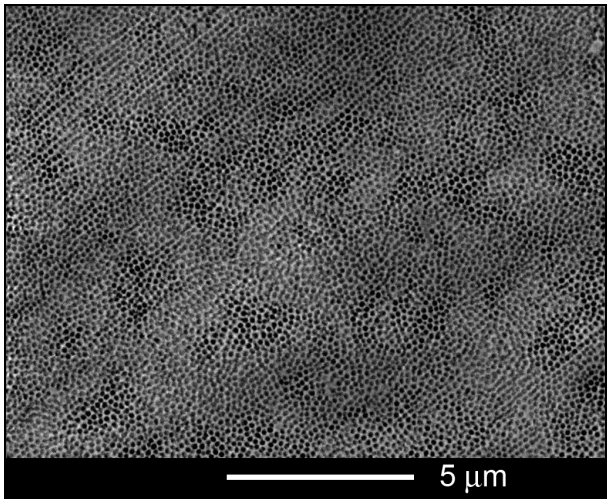

Fig. 1. TiO_2 nanotubes produced by etching of Ti foils in 0.5 wt % aqueous HF solutions.

A mixture of HF and H_3PO_4 solutions in ethylene glycol was shown to be suitable for the preparation of TiO_2 nanotubes with diameters up to 250 nm and length up to 40 mm. For this purpose, the Ti foils were treated under 120 V during 4 hours (see Fig. 2).

3. Raman scattering and XRD analysis

The influence of thermal treatment upon the structural properties of TiO_2 nanotubes was investigated by means of X-ray diffraction analysis and Raman scattering. The analysis of Raman spectra (Fig. 3) demonstrates that the as prepared samples are amorphous. As the temperature of annealing increases to 300°C, an anatase structure is formed. Starting from 500°C, a rutile structure is produced which coexists with the anatase structure. A complete phase transition to the rutile structure occurs at 800°C.

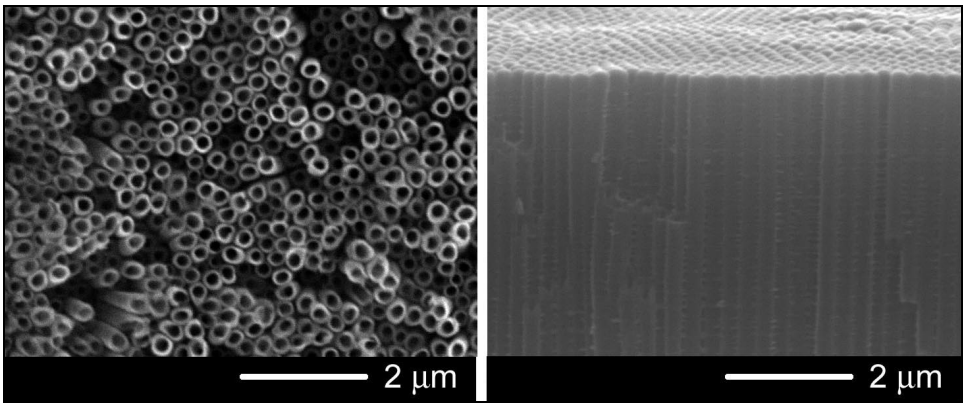

Fig. 2. TiO_2 nanotubes produced by etching of Ti foils in a mixture of HF and H_3PO_4 in ethylene glycol.

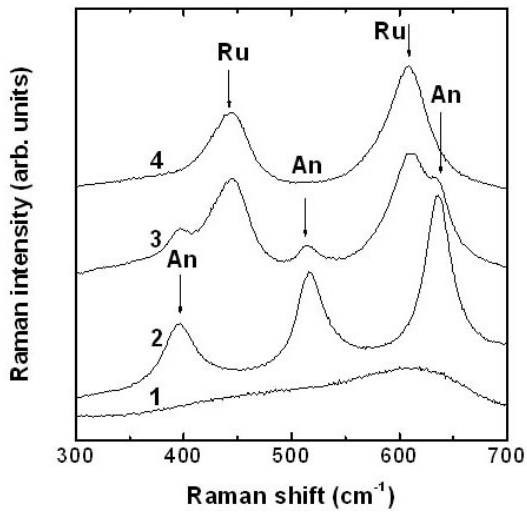

Fig. 3. Raman spectra of TiO_2 nanotubes as-grown (*1*); annealed at 300°C (*2*), 600°C (*3*), 700°C (*4*).

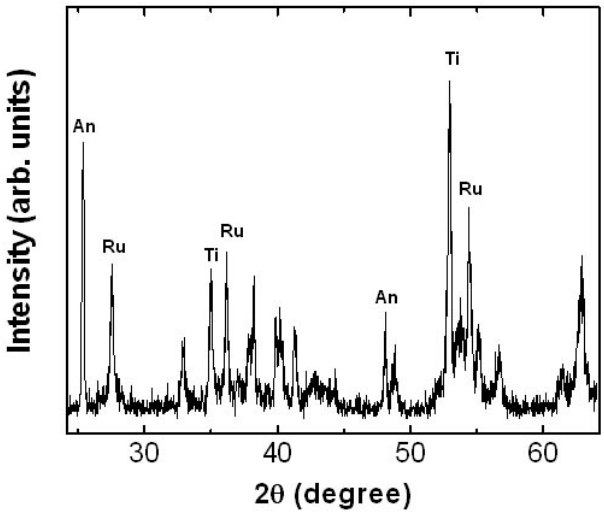

Fig. 4. XRD pattern of TiO_2 nanotubes annealed at 500°C.

Anatase is tetragonal, with two TiO2 formula units (six atoms) per primitive cell. The space group is D_{4h}^{19} (I4/amd). The 18-dimensional reducible representation generated by the atomic displacements contains the zone-center (*k=0)* modes: 3 acoustic modes and 15 optical modes. The irreducible representations corresponding to the 15 optical modes are $1A_{1g} + 1A_{2u} + 2B_{1g} + 1B_{2u} + 3E_g + 2E_u$. Three modes are infrared active, the A_{2u} mode and the two E_u modes. The B_{2u} mode is silent. The remaining six modes corresponding to symmetries $A_{1g} + 2B_{1g} + 3E_g$ are Raman active. The Raman shift for these phonons is 514 cm^{-1} for the A_{1g} mode; 399 cm^{-1} and 514 cm^{-1} for the B_{1g} modes; 144 cm^{-1}, 197 cm^{-1} and 639 cm^{-1} for the E_g modes [14]. Therefore, the A_{1g} and one of the B_{1g} modes overlap. The two E_g modes at 144 cm^{-1}, 197 cm^{-1} are outside of the range of measured Raman shifts.

The rutile structure of titania belongs to the space group D_{4h}^{14} with two TiO_2 molecules per unit cell [15]. The cations are located at sites with D_{2h} symmetry and the anions occupy sites with C_{2v} symmetry. The Ti-ions are surrounded by six oxygen ions at the corners of a slightly distorted octahedron, while the three Ti-ions coordinating each oxygen ion lie in a plane at the corners of a nearly equilateral triangle. According to the factor group analysis,

there are fifteen optical phonon modes with the irreducible representation as given in [16]. There are four Raman active modes with symmetries B_{1g}, E_g, A_{1g}, and B_{2g}. The Raman shift for these phonons is 143 cm^{-1} for the B_{1g} mode, 447 cm^{-1} for the E_g mode, 612 cm^{-1} for the A_{1g} mode, and 826 cm^{-1} for the B_{2g} [17]. The B_{1g} mode at 143 cm^{-1} and the B_{2g} mode at 826 cm^{-1} are outside of the range of measured Raman shifts.

The XRD analysis corroborates the Raman data. The XRD pattern of TiO_2 nanotubes annealed at 500°C (Fig. 5) demonstrates the coexistence of anatase and rutile phases.

4. Characterization of light scattering properties

The photonic strength of the scattering medium is defined in terms of the transport mean free path l_t, which is the average length required to randomize the direction of propagation of the light by scattering. A small value of l_t corresponds to efficient scattering or high photonic strength. The transport mean-free path is given by $l_t = \rho\sigma$, where ρ is the density of scatterers and σ is the transport cross section [18].

To characterize the photonic strength of the samples, the transport mean-free path l_t is deduced from enhanced backscattering EBS measurements [19]. EBS refers to an increase of the reflected intensity from a disordered multiple-scattering sample at exactly the backscattering direction. This increase is due to interference of waves propagating along time-reversed optical paths.

The EBS measurements were performed with a He:Ne laser as light source (λ = 633 nm). The measured angular dependence of the backscattering TiO_2 samples with morphologies illustrated in Figs. 1 and 2, respectively, is shown in Fig. 5.

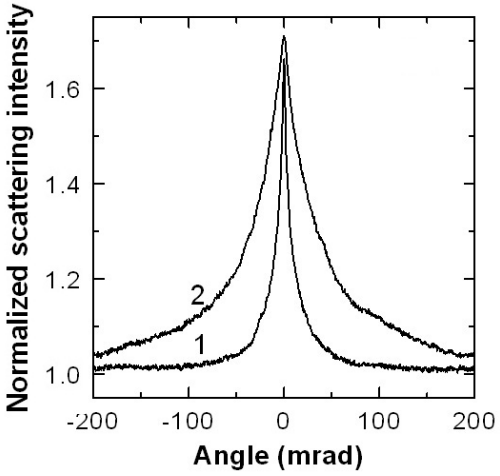

Fig. 5. The measured angular dependence of the backscattering for TiO_2 samples with the morphology illustrated in Fig. 1 (curve *1*) and Fig. 2 (curve *2*).

The full width at half maximum *W* of the EBS cone is directly related to the transport mean free path l_t. For a nonabsorbing and semi-infinite sample, this relation is $l_t = 0.7\lambda(1-R)/2\pi W$ [20], where *R* is the angular and polarization-averaged internal reflection at the sample boundary. The determined value of the transport mean free path is 2.8 μm and 0.6 μm for TiO_2 samples with morphologies illustrated in Fig. 1 and Fig. 2, respectively.

The experiment shows that the transport mean free path decreases with the increase in the average dimensions of pores, indicating therefore the increase in the photonic strength.

5. Photoluminescence study

Photoluminescence (PL) was excited by 351 nm line line of an Ar^+ SpectraPhysics laser and analyzed through a double spectrometer at room temperature. The resolution was better than 0.5 meV. The samples were mounted on the cold station of a LTS-22-C-330 cryostat. Figure 6 presents the PL spectra of TiO_2 nanotubes annealed at different temperatures. The temperature dependence of a sample annealed at 500°C is shown in Fig. 7. The luminescence from both anatase and rutile phases is observed at low temperatures (10 K). For samples annealed at temperatures up to 400°C, the luminescence measured in the spectral range from 370 to 500 nm is dominated by the near bandgap emission from the anatase phase, which includes two narrow lines at 371 nm (3.34 eV) and 372 nm (3.33 eV) followed by several phonon replicas with a phonon energy of 50 meV. The luminescence of samples annealed at temperatures above 700°C comes from the rutile phase and it consists of a near bandgap emission band at 402 nm and a wide blue band with the maximum around 423 nm al low temperatures. The near bandgap emission is quenched with increasing temperature, while the blue band is persistent up to room temperature, it being red-shifted by increasing temperature. Both phases contribute to the low temperature luminescence in samples annealed in the temperature range from 400°C to 600°C, the room temperature luminescence being always determined by the rutile phase.

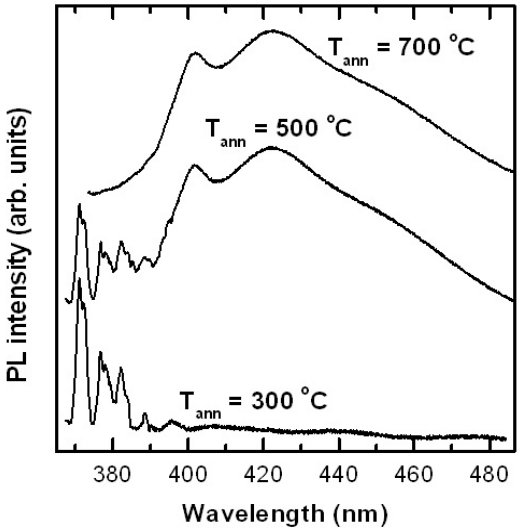

Fig. 6. PL of TiO_2 nanotubes annealed at different temperatures.

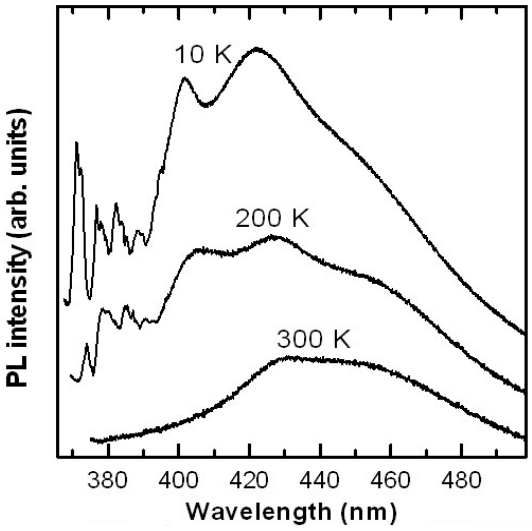

Fig. 7. PL of TiO_2 nanotubes annealed at 500°C measured at different temperatures.

As concerns the nature of the observed PL bands, previously two sharp lines peaking at 3.31 and 3.37 eV have been observed in the near bandgap PL spectra of anatase titania [21]. These lines were interpreted as defect-trapped-exciton related, although the free-exciton origin of the 3.31 eV peak was also argued. Apart from this possible nature of the PL lines at 3.34 eV and 3.33 eV observed in our samples, their relation to free-to-bound transitions cannot be excluded. A band at 402 nm and another one at 439 nm have been previously observed in the cathodoluminescence spectra of rutile phase TiO_2 [22]. The low-temperature photoluminescence spectrum of rutile TiO_2 was found to comprise a peak at 3.031 eV (409 nm), which was attributed to $2p_{xy}$ dipole-allowed second-class excitonic transitions [23]. A band was observed at 450 in the cathodoluminescence spectra of polycrystalline rutile at room

temperature [24]. Previous studies report the presence of shallow traps or deep defect levels associated with the presence of oxygen vacancies which are formed in reduced or oxidized rutile crystals and films [25, 26]. The energies of the shallow traps range from 0.27 to 0.87 eV below the conduction band. Taking this into account, one can suggest that the PL band observed at 402 nm is excitonic, while the band at 423 nm in our rutile samples, as well as the previously observed cathodoluminescence bands at 439 nm and 450 nm, can be attributed to free to bound electronic transitions involving traps below the conduction band.

Conclusions

The results of this work demonstrate the possibility of preparing porous titania templates with controlled morphology and crystallographic structure. The morphology is controlled by the technological conditions of electrochemical oxidation of Ti foils, while the crystallographic structure is controlled by the conditions of thermal treatment. Titania nanotubes with diameters ranging from 30 nm to 250 nm with amorphous, anatase, or rutile structure can be produced. The low temperature luminescence of the produced templates is dominated by excitonic emission and PL bands related to free to bound transitions.

Acknowledgments

This work was supported by STCU under Grant # 4034.

References

[1] W.P. Hsu, R. Yu, and E. Matijevic, Dyes Pigments, 19, 179 (1992).
[2] R.W. Johnson, E.S. Thiele, and R.H. French, TAPPI Journal, 80, 233, (1997).
[3] M. Ferroni, V. Guidi, and G. Martinelli, Nano-Struct. Mater., 7, 709, (1996).
[4] V. Guidi, M.C. Carotta, M. Ferroni, G. Martinelli, L. Paglialonga, E. Comini, and G. Sberveglieri, Sens. Actuators B, 57, 197, (1999).
[5] N. Bonini, M.C. Carotta, A. Chiorino, V. Guidi, C. Malagu, G. Martinelli, L. Paglialonga, and M. Sacerdoti, Sens. Actuators B, 68, 274, (2000).
[6] Z. Ma, Y. Yue, X. Deng, and Z. Gao, J. Molecular Catal. A: Chem., 178, 97, (2002).
[7] U. Bach, D. Lupo, P. Comte, J.E. Moser, F. Weissoertel, J. Salbeck, H. Spreitzer, and M. Grätzel, Nature, 395, 583, (1998).
[8] H.W. Jaffe, Crystal Chemistry and Refractivity, Dover Publications, 265, 1996.
[9] F.A. Hummel, Introduction to Phase Equilibria in Ceramic Systems, Marcel Dekker, 400, 1984.
[10] G.R. Fowles, Introduction to Modern Optics, Dover Publications, New York, 336, 1975.
[11] R. Biswas, M.M. Sigalas, G. Subramania, and K-M. Ho, Phys. Rev. B, 57, 3701, (1998).
[12] V.N. Manoharan, A. Imhof, J.D. Thorne, and D.J. Pine, Adv. Mater., 13, 447, (2001).
[13] V.V. Sergentu, I.M. Tiginyanu, V.V. Ursaki, S. Albu, and P. Schmuki, Physica Status Solidi (RRL), 2, 242, (2008).
[14] T. Ohsaka, F. Izumi, and Y. Fujiki, J. Raman Spectrosc., 7, 321, (1978).
[15] J.H. Xu, T. Jarlborg, and A.J. Freeman, Phys. Rev. B, 40, 7939, (1989).
[16] R. Loudon, Adv. Phys., 13, 423, (1964).
[17] S.P.S. Porto, P.A. Fleury, and T.C. Damen, Phys. Rev., 154, 522, (1966).
[18] A. Ishimaru, Wave Propation and Scattering in Random Media, Academic, New York, 1, 178, 1978.
[19] D.S. Wiersma, M.P. van Albada, and A. Lagendijk, Rev. Sci. Instrum., 66, 5473, (1995).

[20] M.B. van der Mark, M.P. van Albada, and A. Lagendijk, Phys. Rev. B, 37, 3575, (1988).
[21] A. Suisalu, J. Aarik, H. Mändar, and I. Sildos, Thin Solid Films, 336, 295, (1998).
[22] J.-M. Ming, W.-T. Wu, and H.C. Shih, J. Electrochem. Soc., 152, G613, (2005).
[23] A. Amtout and R. Leonelli, Phys. Rev. B, 51, 006842, (1995).
[24] R. Plugaru, A. Cremades, and J. Piqueras, J. Phys.: Condens. Matter, 16, S261, (2004).
[25] A.K. Ghosh, F.G. Wakim, and R.R. Addiss Jr., Phys. Rev., 184, 979, (1969).
[26] A. Rothschild, A. Levakov, Y. Shapira, N. Ashkenasy, and Y. Komem, Surf. Sci. 456, 532, (2003).